

Supporting Information for

Rapid In-situ Growth of High-entropy Oxide Nanoparticles with Reversible Spinel Structure
for Efficient Li Storage

Siyu Zhu^{1,†}, Wei Nong^{1,2,†}, Lim Jun Ji Nicholas¹, Xun Cao¹, Peilin Zhang³, Yu Lu¹,
Mingzhen Xiu⁴, Gang Wu², Shuo-Wang Yang², Zheng Liu¹, Madhavi Srinivasan^{1*}, Kedar
Hippalgaonkar^{1,5*}, Yizhong Huang^{1*}

¹ School of Materials Science and Engineering, Nanyang Technological University, 50 Nanyang Avenue,
Singapore 639798, Singapore

² Institute of High Performance Computing, Agency for Science, Technology and Research, 1 Fusionopolis
Way, Connexis, Singapore 138632, Singapore

³ School of mechanical and electrical engineering, Jiaxing Nanhu University, Jiaxing 314001, China

⁴ Energy Research Institute, Interdisciplinary Graduate Programme, Nanyang Technological University,
Singapore

⁵ Institute of Materials Research and Engineering, Agency for Science, Technology and Research, Singapore
138634, Singapore

* Corresponding authors: madhavi@ntu.edu.sg; kedar@ntu.edu.sg; yzhuang@ntu.edu.sg

† Siyu Zhu and Wei Nong contributed equally to this work

Entropy estimation

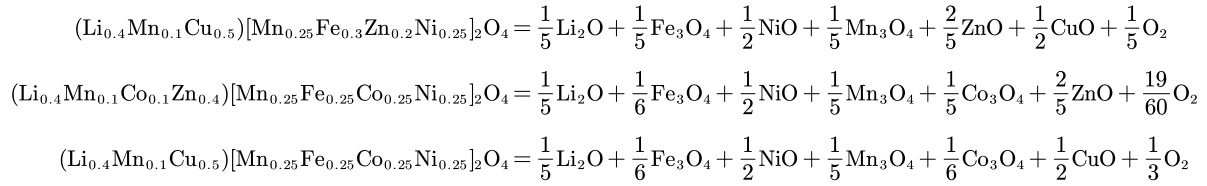
The configuration/mixing entropy (S) of spinel HEO per formula is calculated by the following equation¹,

$$S = -R \sum_{\text{site}} m_{\text{site}} \sum_i^N x_{i,\text{site}} \ln x_{i,\text{site}}, \quad \sum_i^N x_i = 1 \quad \text{Eq. S1}$$

where R is gas constant, m_{site} is the multiplicity per formula of a crystallographic site, and x_i is the molar fraction of element i on the corresponding site, which meets normality.

Stability evaluation

The stability of the HEO is evaluated by the reaction energy (enthalpy) of decomposing HEO phase into the respective most stable mono-metal oxides, ΔH_d , as follows,



the ground states of Li_2O ($Fm-3m$), Fe_3O_4 ($Fd-3m$), NiO ($Fm-3m$), Mn_3O_4 ($I4_1/amd$), Co_3O_4 ($Fd-3m$), CuO ($C2/c$), ZnO ($P6_3mc$), O_2 ($C2/m$) were adopted as references.

Then ΔH_d is calculated by

$$\Delta H_d = \sum_j c_j \cdot E_j - E_{\text{HEO}} \quad \text{Eq. S2}$$

where c_i and E_j are the coefficient and DFT+ U -calculated total energy (per formula) of decomposed product i , E_{HEO} is the DFT+ U -calculated total energy per spinel formula of the corresponding HEO. The ground-state magnetic configurations are used for respective mono-metal oxides, e.g., Li_2O is nonmagnetic, Fe_3O_4 is ferrimagnetic, Co_3O_4 is ferromagnetic, NiO is antiferromagnetic, Mn_3O_4 is ferrimagnetic, CuO is paramagnetic and ZnO is diamagnetic.

Table S1. Metal concentrations (ppb), contents (mol) by ICP-MS method in HEOs samples, and normalized coefficients (x) in one spinel formula (M_3O_4)

Concentration	Co	Ni	Zn	Li	Fe	Mn	Cu
(ppb)							
LFNM-CuZn	—	49.10	48.30	5.01	51.90	58.40	56.40
LFNM-CoZn	32.50	28.10	27.50	3.09	26.70	32.60	—
LFNM-CoCu	38.80	37.70	—	4.66	39.40	42.90	40.30
(mol)							
LFNM-CuZn	—	0.84	0.74	0.72	0.93	1.06	0.89
LFNM-CoZn	0.55	0.48	0.42	0.45	0.48	0.59	—
LFNM-CoCu	0.66	0.64	—	0.67	0.71	0.78	0.63
x in spinel $[M_x]O_4$, $\sum x = 3$							
LFNM-CuZn	—	0.48	0.43	0.42	0.54	0.62	0.51
LFNM-CoZn	0.56	0.48	0.42	0.45	0.48	0.60	—
LFNM-CoCu	0.48	0.47	—	0.49	0.51	0.57	0.46
x in spinel $[M_x]O_4$ used for SQS generation							
LFNM-CuZn	—	0.5	0.4	0.4	0.6	0.6	0.5
LFNM-CoZn	0.6	0.5	0.4	0.4	0.5	0.6	—
LFNM-CoCu	0.5	0.5	—	0.5	0.5	0.6	0.5

Table S2. Entropy estimates for the prepared HEOs

HEO	Reduced formula	S_{config} (R/formula)
LFNM-CuZn	$(Li_{0.4}Mn_{0.1}Cu_{0.5})[Mn_{0.25}Fe_{0.3}Zn_{0.2}Ni_{0.25}]_2O_4$	3.70
LFNM-CoZn	$(Li_{0.4}Mn_{0.1}Co_{0.1}Zn_{0.4})[Mn_{0.25}Fe_{0.25}Co_{0.25}Ni_{0.25}]_2O_4$	3.97
LFNM-CoCu	$(Li_{0.4}Mn_{0.1}Cu_{0.5})[Mn_{0.25}Fe_{0.25}Co_{0.25}Ni_{0.25}]_2O_4$	3.71

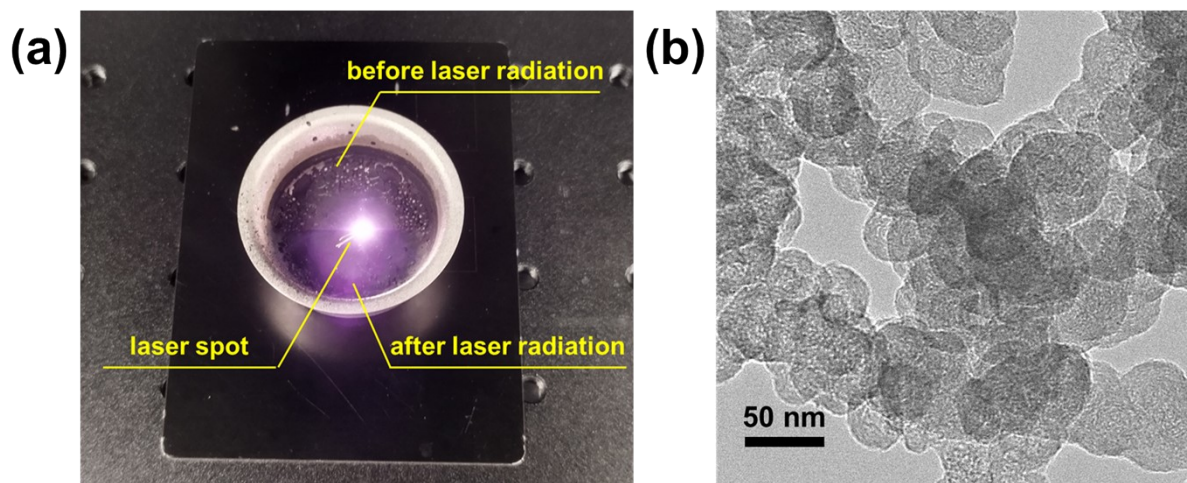


Figure S1. a) Photograph taken during the laser preparation process. b) TEM images of carbon black substrate

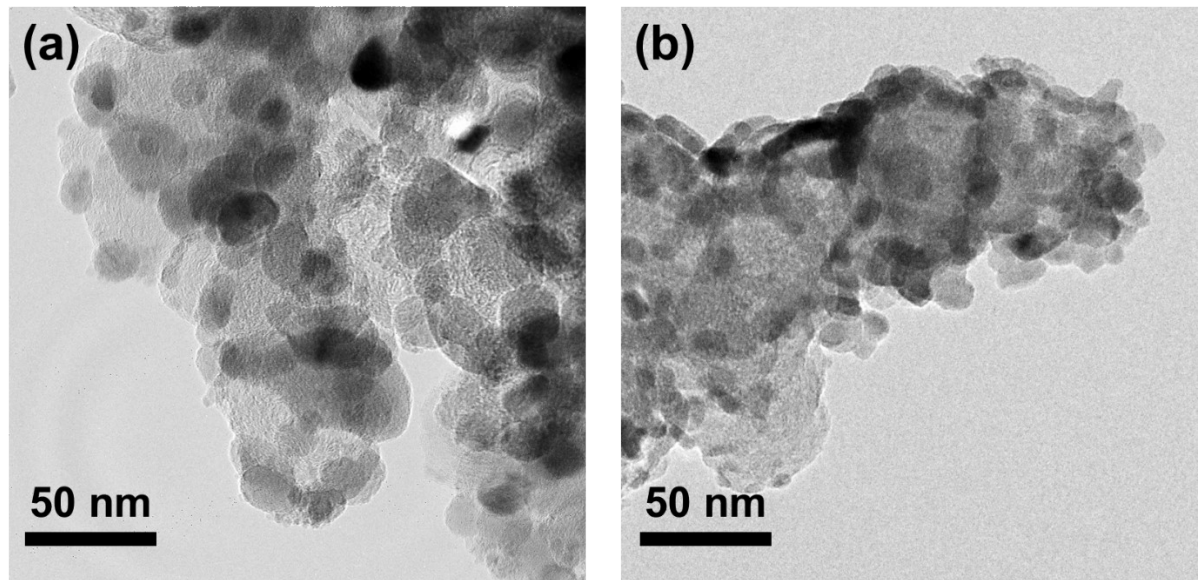


Figure S2. TEM images of a) LFNM-CoCu and b) LFNM-CoZn.

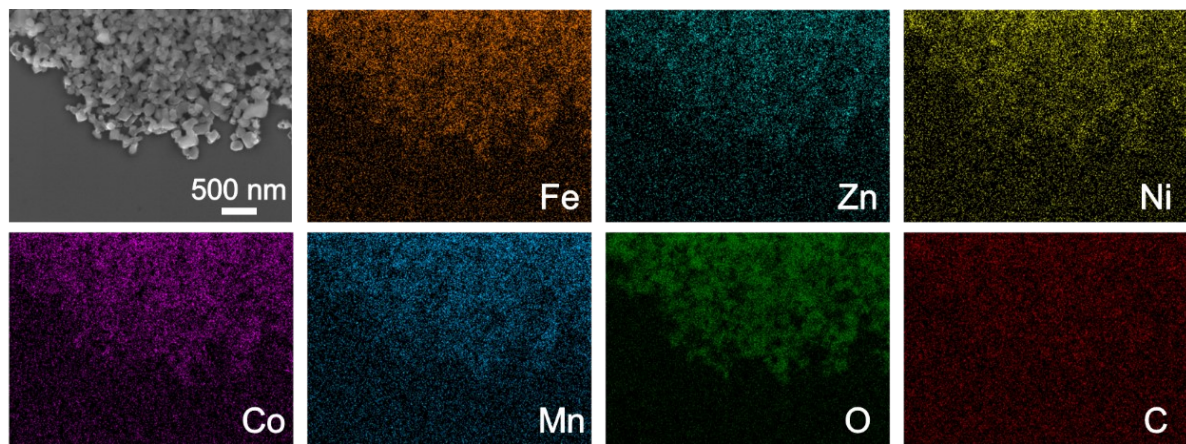


Figure S3. FESEM images and EDX mappings of bulk-HEO after 800 °C annealing process.

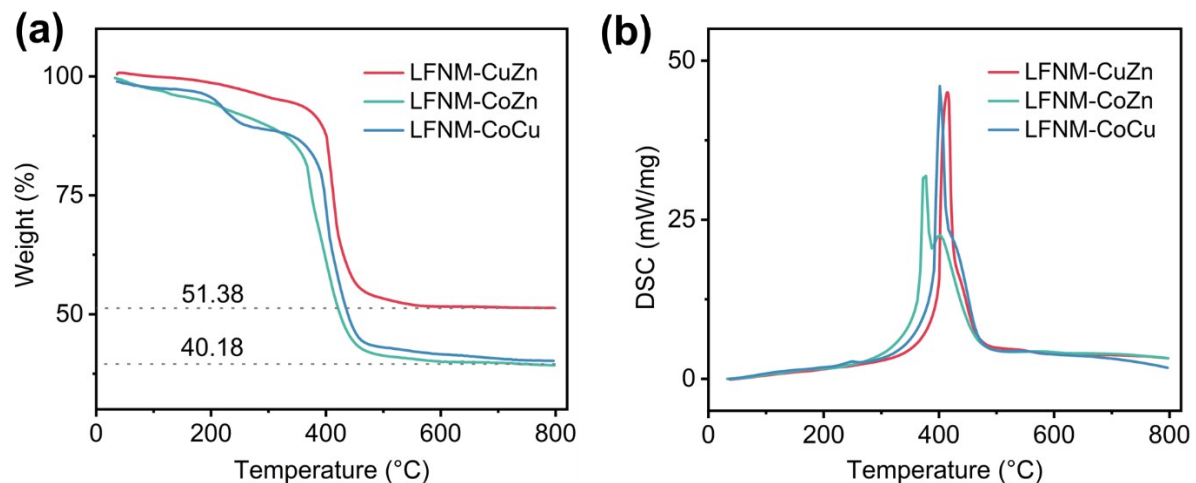


Figure S4. a) TG and b) DSC curves of HEO nanoparticle composite electrode material samples.

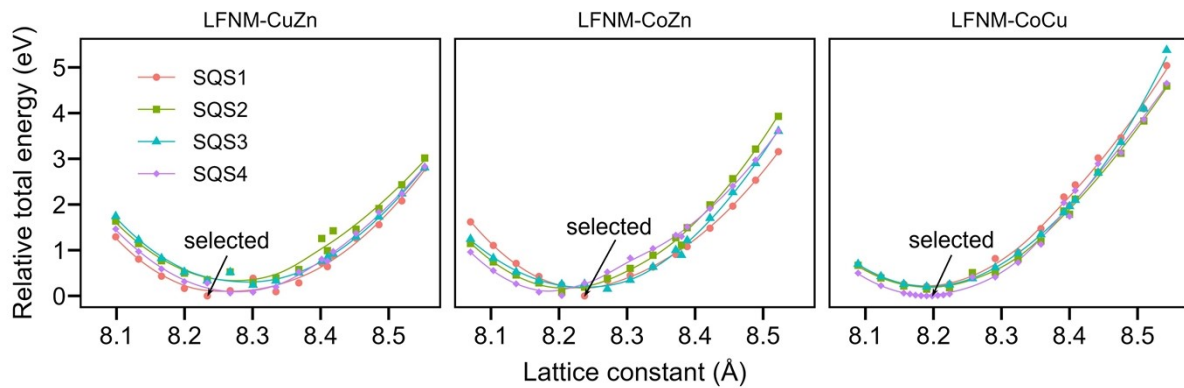


Figure S5. Total energy of SQS as a function of lattice constant of spinel. The relative total energy is referenced to the lowest value in each HEO model.

Table S3. Lattice constant of representative SQS cells as obtained from **Figure S5**

HEO	Calculated Lattice constant (Å)
LFNM-CuZn	8.23339
LFNM-CoZn	8.23754
LFNM-CoCu	8.19819

Table S4. DFT+ U -calculated total energies of metal oxides and decomposition energies of HEOs

Oxide	Z^a	E_{DFT} (eV)	E_{DFT} (eV/formula)	ΔH_d (eV/formula)
Co_3O_4	2^b	−84.962	−42.481	
CuO	4	−39.431	−9.858	
Fe_3O_4	2^b	−93.182	−46.591	
Li_2O	4	−57.253	−14.313	
Mn_3O_4	2^b	−106.650	−53.325	
NiO	8^c	−80.735	−10.092	
ZnO	2	−17.859	−8.929	
O_2	1^b	−9.877	−9.877	
LFNM-CuZn	10	−403.618	−40.362	1.99
LFNM-CoZn	10	−426.354	−42.635	1.10
LFNM-CoCu	10	−419.748	−41.975	0.33

^a Z : the number of formula units in the calculated unit cell.

^b The primitive cell was used in the calculations.

^c A $2 \times 2 \times 2$ supercell of the primitive cell was used to obtain antiferromagnetic configuration.

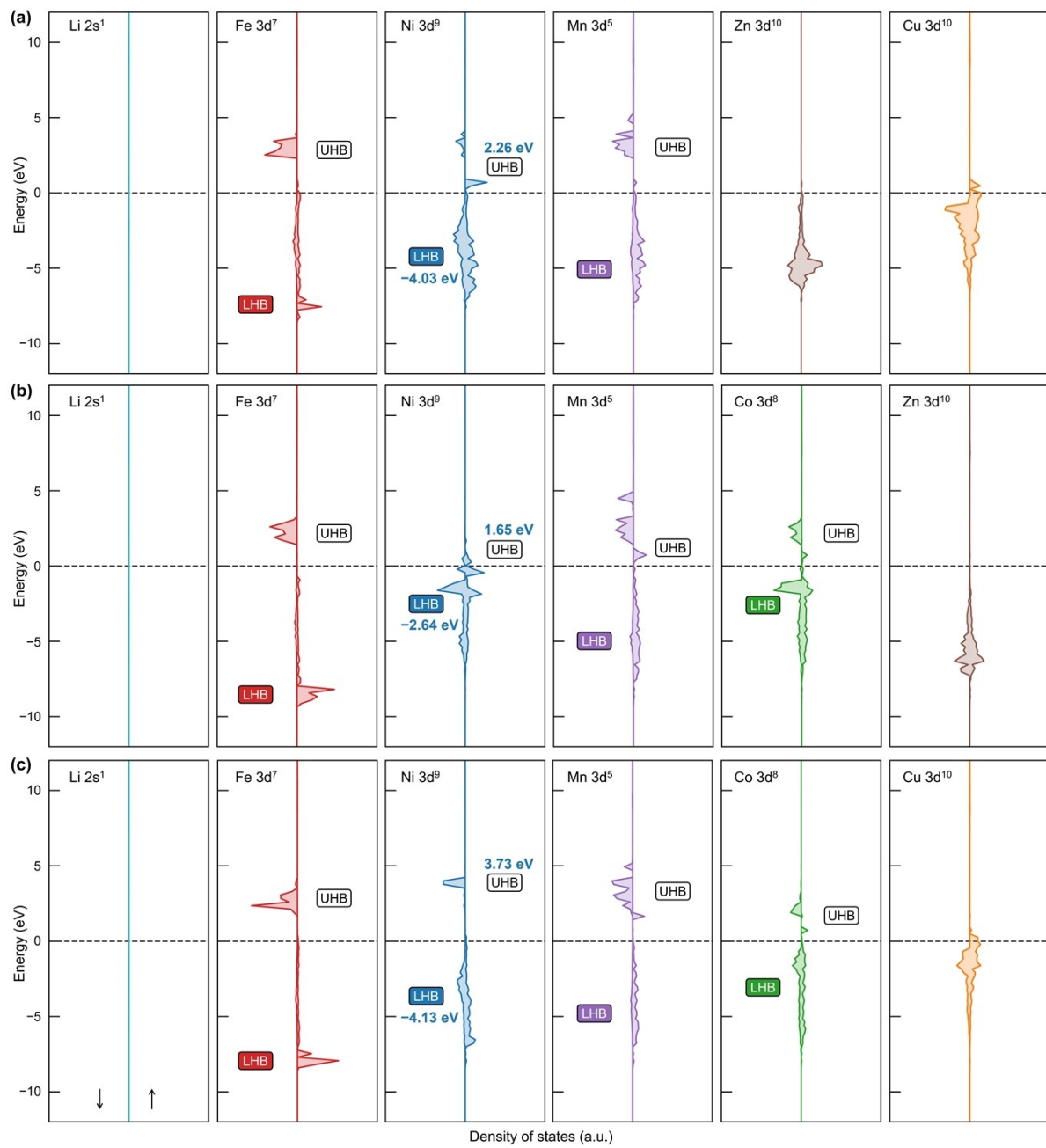


Figure S6. Metal-projected DOS of (a) LFNM-CuZn, (b) LFNM-CoZn, and (c) LFNM-CoCu.

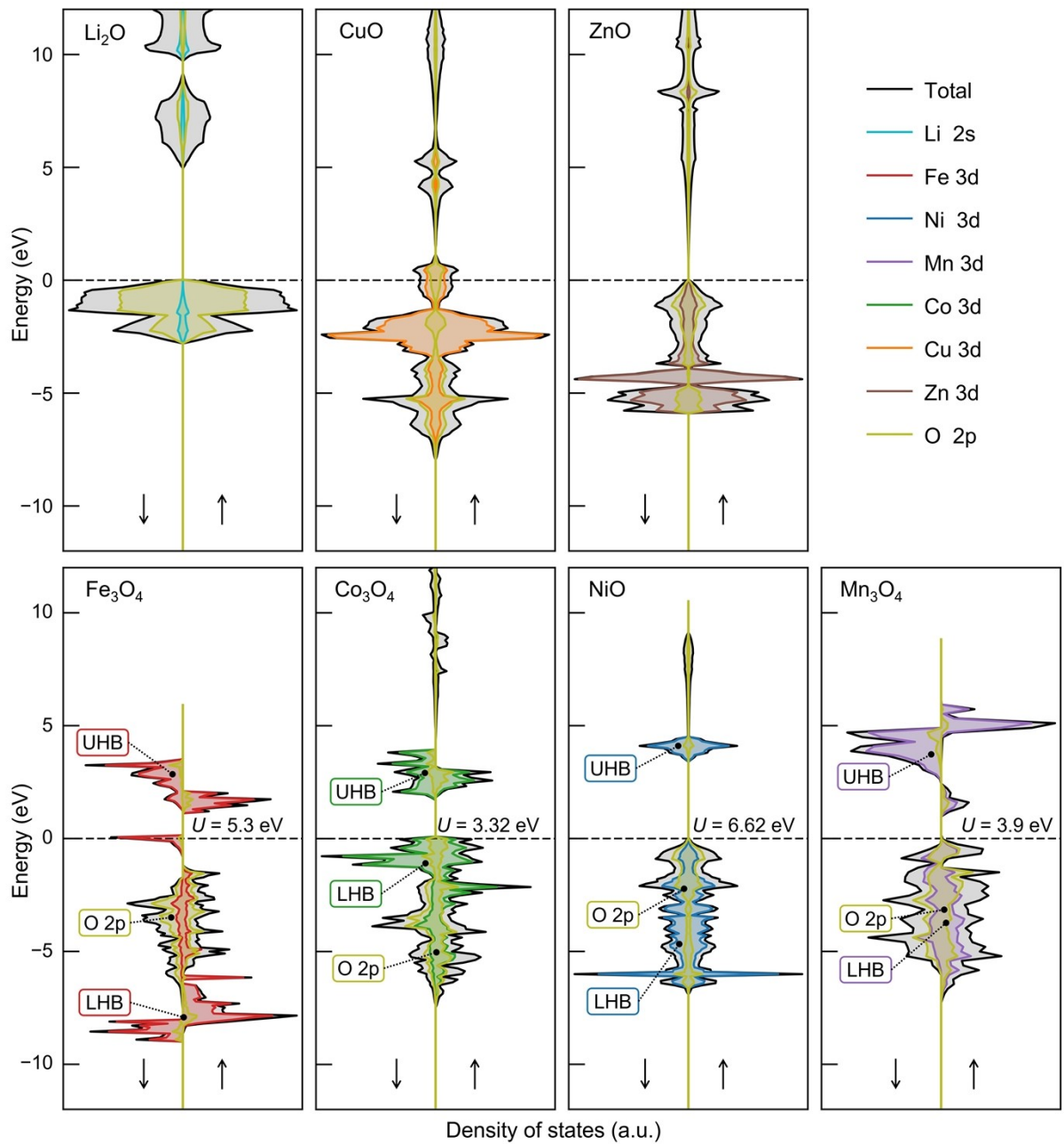


Figure S7. DOS of metal-oxides. The first row was obtained from pure DFT (PBE) calculations, while the second row from DFT+ U calculations, and the lower Hubbard band (LHB) and upper Hubbard band (UHB) of metals, and O 2p bands are indicated. The Fermi energy is set at 0 eV.

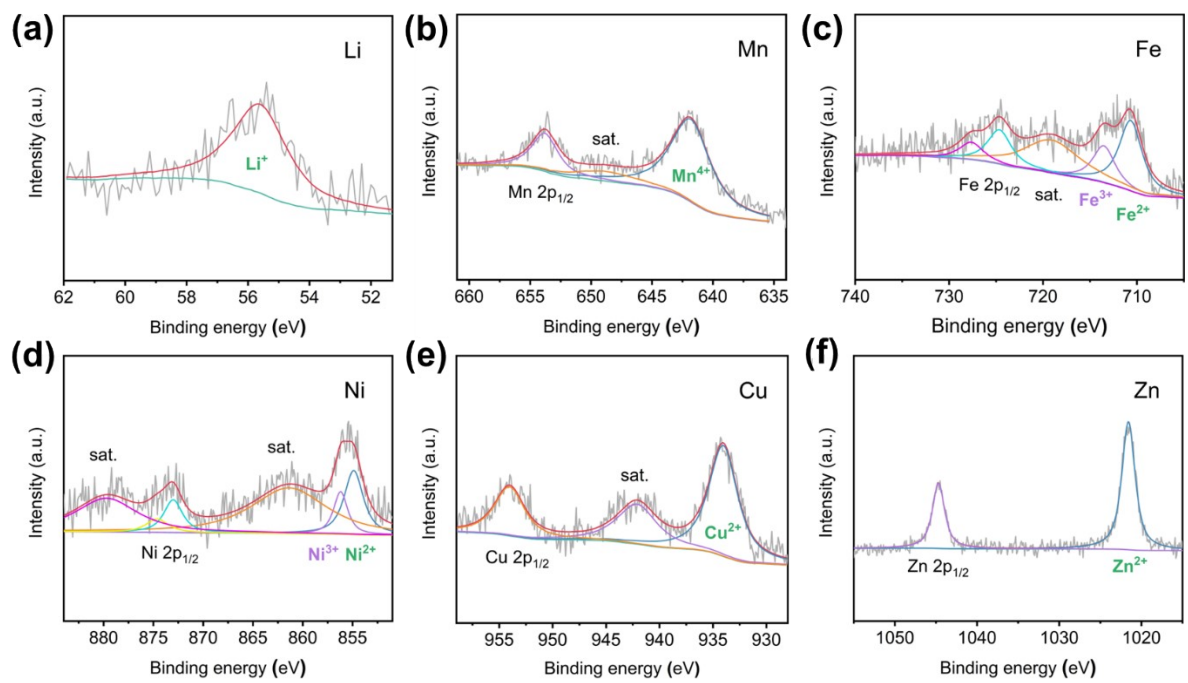


Figure S8. XPS a) Li 1s, b) Fe 2p, c) Ni 2p, d) Mn 2p, e) Cu 2p, f) Zn 2p spectra of LFNM-CuZn sample.

Table S5. The comparison of HEO anodes with alkali-metal and without cobalt

Material	Cycling performance	High-rate performance	Reference
HEOs with alkali-metal			
(MgCoNiCuZnLi)O	417 mAh g ⁻¹ after 300 cycles @ 1.0 A g ⁻¹	301 mAh g ⁻¹ @ 5.0 A g ⁻¹	²
(MgCoNiZn) _{0.65} Li _{0.35} O	610 mAh g ⁻¹ after 100 cycles @ 1.0 A g ⁻¹	680 mAh g ⁻¹ @ 1.0 A g ⁻¹	³
(FeCoNiCrMnZnLi) ₃ O ₄	522 mAh g ⁻¹ after 100 cycles@ 0.05 A g ⁻¹	173 mAh g ⁻¹ @ 2.0 A g ⁻¹	⁴
(FeCoNiZnMnLi) ₃ O ₄	605 mAh g ⁻¹ after 100 cycles@ 0.1 A g ⁻¹	225 mAh g ⁻¹ @ 2.0 A g ⁻¹	⁵
(CrCoNiZnMnLi) ₃ O ₄	460 mAh g ⁻¹ after 100 cycles@ 0.1 A g ⁻¹	145 mAh g ⁻¹ @ 2.0 A g ⁻¹	⁵
Li _{1.8} (FeCoZnCrMn) ₃ O _x	484 mAh g ⁻¹ after 300 cycles@ 0.5 A g ⁻¹	146 mAh g ⁻¹ @ 1.0 A g ⁻¹	⁶
Li _{0.1} (LiLaCaSrBa) Ti _{0.9} Al _{0.1} O ₃	57 mAh g ⁻¹ after 100 cycles@ 0.1 A g ⁻¹	37 mAh g ⁻¹ @ 1.0 A g ⁻¹	
HEOs without cobalt			
(FeNiCrMnZn) ₃ O ₄	387 mAh g ⁻¹ after 185 cycles @ 0.5 A g ⁻¹	300 mAh g ⁻¹ @ 2.0 A g ⁻¹	⁷
(MgTiZnCuFe) ₃ O ₄	504 mAh g ⁻¹ after 300 cycles @ 0.5 A g ⁻¹	272 mAh g ⁻¹ @ 2.0 A g ⁻¹	⁸
(CrMnFeNiCu) ₃ O ₄	~632 mAh g ⁻¹ after 250 cycles@ 0.5 A g ⁻¹	451 mAh g ⁻¹ @ 2.0 A g ⁻¹	⁹
(CrMnFeNiCu) ₃ O ₄	~691 mAh g ⁻¹ after 200 cycles@ 0.5 A g ⁻¹	480 mAh g ⁻¹ @ 2.0 A g ⁻¹	¹⁰
(CrMnFeNiZn) ₃ O ₄	~668 mAh g ⁻¹ after 200 cycles@ 0.5 A g ⁻¹	560 mAh g ⁻¹ @ 3.0 A g ⁻¹	¹¹
(LiFeNiMnCuZn) ₃ O ₄ nanoparticles	865 mAh g ⁻¹ after 800 cycles@ 0.5 A g ⁻¹	585 mAh g ⁻¹ @ 2.0 A g ⁻¹ , 436 mAh g ⁻¹ @ 5.0 A g ⁻¹	This work

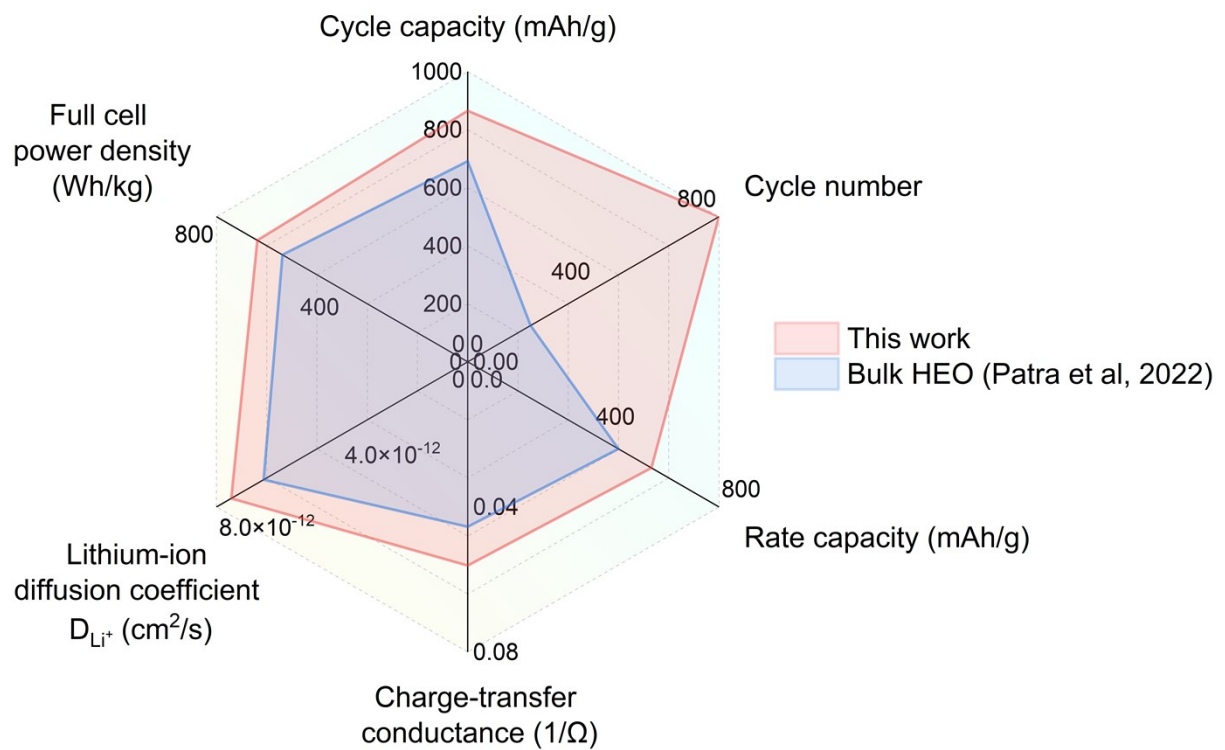


Figure S9. The comprehensive comparison of the performances between the LFNM-CuZn HEO nanoparticle anode (this work) and a state-of-the-art bulk-HEO anode¹¹.

Table S6. R_b , R_{sei} and R_{ct} values of various electrodes by fitting the Nyquist plots

	R_b (Ω)	R_{sei} (Ω)	R_{ct} (Ω)
LFNM-CuZn	14.2	34.0	17.8
LFNM-CoZn	22.3	53.7	26.4
LFNM-CoCu	13.3	39.2	29.4
bulk-HEO	6.33	12.0	35.9

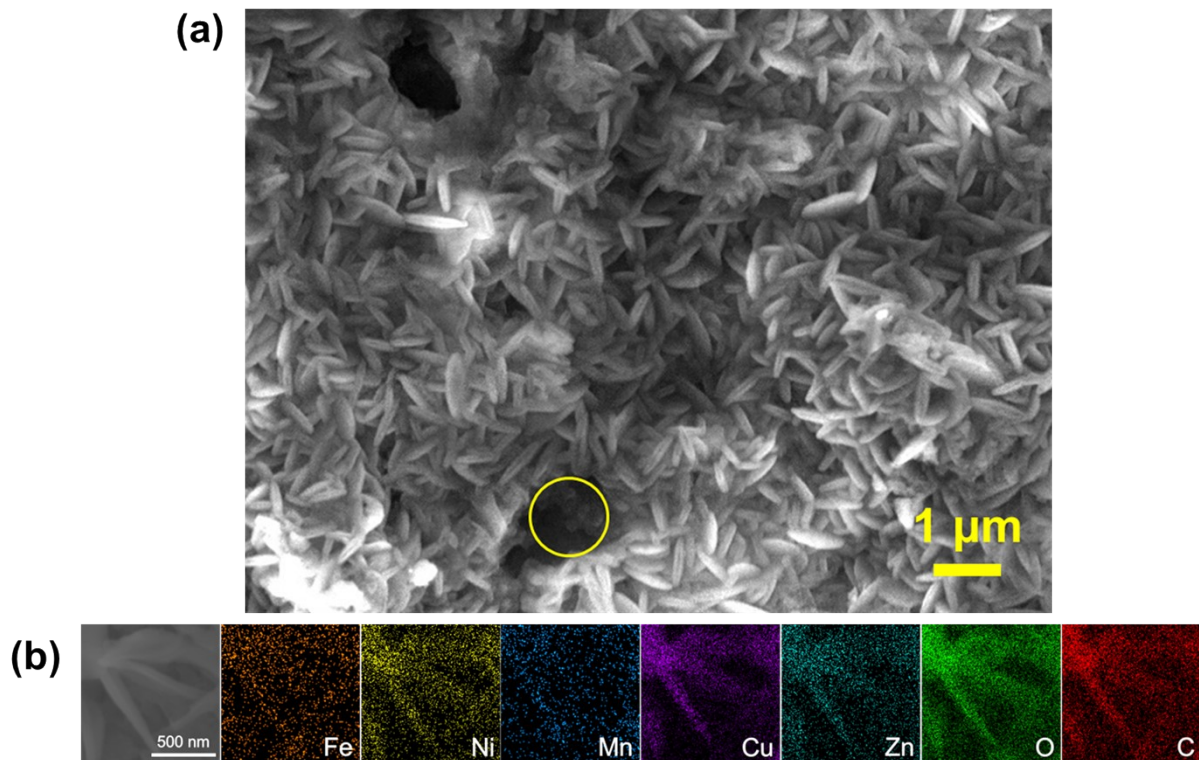


Figure S10. a) The SEM image of HEO nanoparticle anode in LIB after 200 cycles. b) The EDX-mapping images regarding Fe, Ni, Mn, Cu, Zn, O and C elements of the electrode after 200 cycles.

Table S7. Specific capacity limit of HEO nanoparticle anodes for the various stage of Li insertion

HEO nanoparticle anodes	$x_1(\text{Li})$	C_1	$x_2(\text{Li})$	C_2	$x_3(\text{Li})$	C_3
(Li _{0.4} Mn _{0.1} Cu _{0.5})[Mn _{0.25} Fe _{0.3} Zn _{0.2} Ni _{0.25}] ₂ O ₄	1	125	2	249	9	1,122
(Li _{0.4} Mn _{0.1} Co _{0.1} Zn _{0.4})[Mn _{0.25} Fe _{0.25} Co _{0.25} Ni _{0.25}] ₂ O ₄	1	123	2	245	9	1,104
(Li _{0.4} Mn _{0.1} Cu _{0.5})[Mn _{0.25} Fe _{0.25} Co _{0.25} Ni _{0.25}] ₂ O ₄	1	123	2	246	9	1,105

[^] x and C (mAh g⁻¹) indicate the molar ratio of inserted Li w.r.t the spinel formula and the specific capacity, respectively. 1, 2, and 3 denote the three stages of lithiation.

The spinel oxides, such as LiMn₂O₄ and Li₄Ti₅O₁₂, can serve as Li insertion materials due to their specific oxidation states and structure stability. However, their specific capacities are limited by factors such as the Jahn-Teller distortion and the max amount of inserted Li. The high-entropy oxides (HEOs, AB₂O₄) show improved specific capacities (~400 to ~700 mAh g⁻¹, Table S5) due to the involvement of additional Wyckoff sites for Li insertion. The chemical reactions during HEO (de)lithiation, which maintain the spinel structure whereby providing high specific capacity, are yet to be clearly revealed. Nevertheless, three stages of lithiation are suggested as the Li insertion mechanism for the spinel HEOs. During stage 1, half of the empty octahedral voids are filled with Li, resulting in a specific capacity of ~125 mAh g⁻¹:



where V_{8a} is the 8a tetrahedral vacancies that generate by ion displacement from 8a site to 16c site due to the Coulomb interaction. During stage 2, the generated empty tetrahedral voids are re-occupied, doubling the specific capacity:



During stage 3, all possible empty tetrahedral voids could be involved, leading to a specific capacity of ~1, 100 mAh g⁻¹:



These stages involve specific chemical reactions that maintain the spinel-like framework of the anode materials leading to high specific capacity, which might be benefited from the co-existence of multiple transition metals with mixed oxidation states, resulting in mitigating the Jahn-Teller distortion and preserving structure stability.

Appendix

1. The relaxed atomic positions of SQS cell for LFNM-CuZn (in POSCAR format), where the Tc denotes the Mn atoms in tetrahedral sites.

LFNM-CuZn							
8.233390000000000							
Cu	Fe	Li	Mn	Ni	O	Tc	Zn
5	6	4	5	5	40	1	4
Direct							
0.0630521061071434	0.4554578442647212	0.1415337105793171					
0.4760013292346201	0.8429731975286145	0.9558584694750039					
0.7296893426952806	0.3493653820527456	0.4491271990243746					
0.1278805523414803	0.7509608679954169	0.2504634970974209					
0.9205817473219042	0.5486158360914928	0.8538634148209994					
0.1054218737905686	0.0950248073193549	0.1961315371186103					
0.5893565726215897	0.6052046716416370	0.6960253801967653					
0.7943156019140076	0.8066130295402161	0.1073953993955641					
0.5938394366105726	0.0977327902321150	0.7006362758964002					
0.7996783901854272	0.8028126234913202	0.5967704396259066					
0.0046912786697391	0.9977639124980371	0.9984096704971464					
0.5255708129818331	0.1510185783626952	0.0508909173379095					
0.3276710679540287	0.9472878240195115	0.6485173441697683					
0.6745522736405505	0.0514700929898879	0.3488212886644675					
0.2738764157404248	0.6510704223408084	0.5480254489388514					
0.3932842499223810	0.4026425420782687	0.8005612288623212					
0.3995570854766086	0.4013522041739321	0.2997264278853606					
0.0019117276920326	0.4994944146951710	0.4947473705069996					
0.9030951401962710	0.8935465961829934	0.8026124685074620					
0.2096960689503575	0.1959312731452272	0.3917479772204260					
0.2073358760158115	0.1990996623226451	0.8984016648984863					
0.1975948611817273	0.7000445671520552	0.8974538156757390					
0.4041094452937628	0.9022733030009178	0.3010214011540171					
0.6943569204440436	0.7057009224987425	0.4000697806636495					
0.5936990595981726	0.6060441357429340	0.2081302641861953					
0.7371537995800779	0.5064836534026540	0.0211429650008697					
0.6253925492385406	0.4111016575708746	0.7992716947280911					
0.8519454861177778	0.5930283180517080	0.6822460546077238					
0.0567586563450249	0.3047259232607615	0.5732639243286144					
0.9397281157665276	0.7142037178548080	0.9099710823628087					
0.5395235700778258	0.3148272093101241	0.1147257194895204					
0.6672858112969635	0.8982121271255608	0.7938449958038731					

0.4382776836209672	0.2117154615002121	0.8869190790852741
0.2422120403967014	0.0060485678054718	0.0017958155407882
0.3426437304387520	0.0889964728426449	0.2154059203182186
0.5463983908860044	0.8072676125849583	0.1201279845625649
0.7719591875860843	0.9874446187759318	0.9904111798784356
0.8448861092605995	0.0804127505847703	0.7093812603157943
0.4479367377496644	0.6937271800047355	0.8892938864739506
0.9787966299979161	0.1968489446837367	0.3857107830929607
0.6347406466657759	0.8954235375127553	0.2965903584264638
0.5452481375630924	0.2978831920949290	0.6171248395794464
0.0717018481172076	0.2813625536044313	0.0875719847119214
0.1740265409017212	0.9057537583304622	0.2971579230003982
0.2564015557442190	0.5025725570280883	0.9826379677460082
0.0411826890642999	0.8036127599724168	0.0940322738323687
0.8278206648884492	0.6146312511501435	0.2120312795169781
0.9391990881576220	0.6901946164363792	0.4085138745539183
0.1566119351675468	0.3964804322288416	0.3091246049259482
0.3641096319095425	0.5894818095225958	0.2092980492854863
0.7469123114348832	0.9967777126466189	0.5150446269043130
0.3469428520814333	0.1091303650354831	0.7153851605688075
0.4591599838222180	0.7202542807198284	0.3855661915661912
0.2380138675997330	0.4926312105167909	0.4869225324424633
0.0264622776394248	0.8023093184769934	0.6186610757412652
0.1291445468800276	0.8946404088762065	0.8084628142249528
0.3567216076102895	0.5872344482105163	0.7091052122533412
0.5708614831093044	0.7855919246397534	0.5916822595264506
0.9751555801881295	0.1934820746734260	0.9059842219645375
0.7599182252974828	0.5095127947893303	0.5007445466489244
0.8761931656564172	0.0946020254608868	0.1890679537854467
0.6237754396210988	0.4087439984008725	0.3043707515478502
0.4303351413819030	0.2148096426911579	0.3906527008920762
0.2574904575711088	0.0093147729136049	0.4766830434342850
0.1670816927584724	0.3939454332948671	0.7975205805171299
0.8761765064062388	0.2478545046645664	0.7528715878498744
0.3058618771980761	0.2947726430057287	0.5968993394550139
0.0042694938140926	0.9925387943801809	0.5011244522210703
0.4985502171976819	0.5018400856977223	0.0031796162877242
0.7982127996127275	0.2980713763040157	0.1055334386006663

2. The relaxed atomic positions of SQS cell for LFNM-CoZn (in POSCAR format), where the Rh and Tc denote the Co and Mn atoms in tetrahedral sites, respectively.

LFNM-CoZn									
8.237540000000000									
1.000000000000000					0.000000000000000			0.000000000000000	
0.500000000000000					1.000000000000000			0.500000000000000	
0.500000000000000					-0.500000000000000			1.000000000000000	
Co	Fe	Li	Mn	Ni	O	Rh	Tc	Zn	
5	5	4	5	5	5	40	1	1	4
Direct									
0.8979305427991551	0.9052996436451193	0.7970323383663035							
0.3036958406335595	0.2972524888565971	0.5960067259725158							
0.2039958130276708	0.2002670535186084	0.4024378764079869							
0.3951686058171624	0.3987987060989731	0.3046317988080574							
0.3960495661242223	0.9040240014545868	0.3052520754812144							
0.2012275138034148	0.7031315375256747	0.8866899881509511							
0.5840318045297582	0.5998606651677105	0.2194061701397943							
0.7932571676369489	0.8019358455310052	0.1039647925899737							
0.0029324110566913	0.0119153300159112	0.5015318629444132							
0.8064963015042299	0.8010714425290005	0.5985307879665754							
0.7260495215162478	0.3419609932996087	0.4538118652686129							
0.8759958563423796	0.2515318951244566	0.7421180637175241							
0.2730825314615125	0.6534006899324813	0.5535489644549145							
0.3327038249883681	0.9455679353637739	0.6414662887845682							
0.7956650197792235	0.2990079073959206	0.1033331796232604							
0.6074859621087552	0.5941857360725381	0.6959249329633928							
0.0018237264403077	0.0025002304891803	0.9924379486534998							
0.4968372714485495	0.4996643525813181	0.9997539384701397							
0.2035096655802432	0.1983034329769867	0.8897121609750487							
0.6973021856967243	0.6982210687823313	0.4048847033744568							
0.0070829973222180	0.4915292291537151	0.5043079633408719							
0.5964926424487044	0.0997666525003413	0.6966848355100909							
0.1018509728167390	0.1022188638909502	0.2017033934157615							
0.4058857842053364	0.3996638660300205	0.7923322522990222							
0.5254341784471819	0.3202566088636820	0.1067232577662658							
0.4586790751160778	0.6830366347525487	0.8923805627372340							
0.6569390457462236	0.9080269677075120	0.7860185756935713							
0.6510446159787577	0.8918719029985752	0.2951637578744617							
0.2270074156561789	0.0145602785975004	0.9939059590087683							
0.3393926827818729	0.0990821277622767	0.2181512547354205							
0.5452483988311672	0.7994493403989905	0.1207361117191730							
0.7737070557261140	0.9912938274907848	0.9882764333244067							
0.8297003572799827	0.0931312985001281	0.7016634130079700							
0.9480005163730796	0.7115004452020066	0.9037484123946313							

0.0783157136169800	0.3004859577327172	0.5832380494073508
0.8476551528701471	0.5978298433696251	0.6861768690363877
0.6361425455771411	0.4178705303721182	0.8098785330213825
0.7275293804648107	0.4932773368344941	0.0182129924478873
0.4427381959194990	0.1953311052502939	0.8828335861546542
0.9776515386130458	0.1958379147371404	0.3980048546704151
0.1699487616798926	0.3780062801425344	0.7890412390049000
0.5316436444833087	0.2860622786810392	0.6109481175510386
0.0670907841379897	0.2861177508282317	0.0773320176761866
0.1489464441531605	0.9113067927059945	0.3100867743055511
0.2679846345010399	0.5105324277106547	0.9869003971671326
0.0452118342722329	0.8123280708378426	0.0818600809509639
0.8236768758207421	0.6145554543876012	0.2124987794345367
0.9367939885917611	0.6850370834539633	0.4135612596657193
0.1597622431675540	0.3922529544811281	0.3252684458149864
0.3627749529941420	0.5823097087823956	0.1965282974802096
0.2509813529814110	0.4791896296716414	0.4951485899610776
0.3553474282300935	0.1141570382316577	0.6976668273926530
0.7524395866933354	0.0006835013304903	0.5135034183647467
0.2540408349952034	0.0097777796847465	0.4809591950518279
0.4618312939062038	0.7090234513118662	0.3975020643344094
0.1360642381120080	0.9033256849736767	0.8125055313351690
0.3720451235505561	0.5980742066016349	0.7044433344007857
0.5752153962636066	0.7766518635324317	0.5967932636874973
0.9611544722422354	0.1932892326949750	0.9084771026653738
0.7625997142097051	0.5013606981061719	0.5139398379197151
0.8607116402449922	0.1048142723259681	0.1779851162994260
0.6345425869434103	0.3980571604718033	0.2915924697857821
0.4245769413932634	0.2203792318987348	0.4052682945574178
0.0275084974657150	0.8178191134039346	0.6130270664412522
0.5192681425134116	0.1486168768310772	0.0486749962338970
0.0785812315667687	0.4467592462600646	0.1567093009685729
0.9264307158197109	0.5433725481750561	0.8515640764090980
0.6675812250915560	0.0566963726338775	0.3526721420433714
0.4737535832815377	0.8520425571993400	0.9527865679436216
0.1197524326071127	0.7534790441422200	0.2521378644741719

3. The relaxed atomic positions of SQS cell for LFNM-CoCu (in POSCAR format), where the Tc denote the Mn atoms in tetrahedral sites, respectively.

LFNM-CoCu							
8.198190000000000							
1.000000000000000				0.000000000000000			0.000000000000000
0.500000000000000				1.000000000000000			0.500000000000000
0.500000000000000				-0.500000000000000			1.000000000000000
Co	Cu	Fe	Li	Mn	Ni	O	Tc
5	5	5	4	5	5	40	1
Direct							
0.9962835907834399	0.0004118096501619	0.0026148207047680					
0.8021351406737727	0.8013249268999552	0.1001197841216871					
0.9000675310818993	0.8967812464276320	0.8069477237860730					
0.0010735044130555	0.4981149663128451	0.4994785165102820					
0.2953454756446689	0.3010840264959180	0.6026398006159636					
0.4796979364705312	0.8479343196911463	0.9523514572019115					
0.1313589562206335	0.7476590259175938	0.2433674291724092					
0.7210926083214361	0.3412126911674262	0.4564121184903682					
0.5241642422505838	0.1536045933599701	0.0472820089877338					
0.2837069975582467	0.6455327582376239	0.5449849300645150					
0.3840010169139916	0.4072602206194688	0.8062070572332308					
0.4017540993559984	0.9027516190434394	0.3015715749242083					
0.3965444814192453	0.4021722087572016	0.3015729881355792					
0.8038705783296783	0.7995612510464913	0.6004005153990105					
0.9992435756450986	0.9972601091742573	0.4988909450648591					
0.6745329256710998	0.0510275302064233	0.3520242674055287					
0.9161513469464949	0.5507174124016440	0.8530344466725317					
0.0790405548173274	0.4501974865833429	0.1469305989927153					
0.3220992669629045	0.9520577042476650	0.6502999382144173					
0.6020651153701853	0.6024109063113826	0.6974057009152536					
0.2019769396571755	0.2031295434345247	0.4002029765097126					
0.2002725666737472	0.1995219992995523	0.8961902146452131					
0.8015050698530252	0.2999244922229061	0.1021460142287523					
0.7101975077633554	0.6966410211396799	0.3937849392115938					
0.6083464532125835	0.5981213070325335	0.1964590345730157					
0.0995552624957887	0.1007558597527961	0.1983382422668597					
0.4999059026068831	0.5022869179001908	0.9995161843592768					
0.1979687995007042	0.7032515039668106	0.9016945065419263					
0.5957813333157190	0.0968058334765366	0.6967409050633053					
0.7376140473068490	0.4859366732353941	0.0124376637392784					
0.8497941684497131	0.0745668053486392	0.7036889955587028					
0.2286203683218904	0.0105962939225203	0.9943047070973202					
0.3374009242235069	0.1023764574550684	0.2164610390140216					
0.5685208818989033	0.8021530592634231	0.1089908663035220					

0.6762353652575637	0.8966408442287460	0.7936831885357563
0.5604631003978489	0.3081645199003580	0.1040684131670800
0.4571323294339781	0.6922489554156606	0.8847732572369117
0.7705907672416642	0.9854614587123853	0.9983655323940352
0.6292101038384160	0.4183723491190389	0.7958384799162568
0.8439253164603638	0.5970637962999040	0.6834631643216503
0.0682129074209366	0.3082765082065999	0.5835595137550111
0.4333106857337547	0.2036646052372781	0.8896545494707414
0.9346979001415254	0.7240093183140840	0.9128281738792924
0.6625952113816483	0.8794229277080041	0.2925389727572422
0.7624019164227275	0.9901648710748422	0.5076528327714802
0.0460421581639012	0.2900419475749182	0.0869005443501940
0.1608291706959757	0.9062417917549977	0.3018719327984198
0.2673415508599032	0.5054439554577542	0.9887559659570135
0.0257352071750374	0.8176170128585016	0.0945781518681307
0.8384163031747495	0.6198409249977229	0.2012921412334050
0.9428006045817352	0.6856583724145283	0.4092811242230371
0.1506877547439499	0.3945518198078770	0.3175868330222743
0.3674205877814882	0.5896246301826198	0.1988477758488653
0.2361388601038051	0.4866517578988619	0.5031921917800259
0.3359791596562166	0.1200737068276481	0.7054122126143794
0.4753659311139652	0.7021919197716038	0.3906159196889251
0.1609692890321963	0.3832107404781353	0.7955275314665605
0.2437324354915929	0.0114314287466677	0.4869785981670855
0.0358550817219082	0.8080244541090215	0.6139780277440609
0.1131227543510574	0.9100187178046362	0.8202244740517431
0.3628825711441765	0.5989085658474889	0.7065694322823471
0.5732962537739025	0.7822449698101365	0.5894032877453802
0.9560244190969721	0.1930286488018131	0.9169960741168746
0.7574390788583922	0.5124267311229649	0.5011660714297973
0.8609302824753445	0.1036280988347616	0.1786960703448731
0.6514746442019737	0.3952071584777708	0.2871498910942824
0.4231314771733165	0.2139087486115919	0.4116084564092597
0.5184880602708323	0.3020558663528293	0.6121809990634975
0.9716644742680621	0.1915378128956297	0.4009978599113754
0.8737671162289894	0.2477954843404180	0.7482694428572025

Reference

1. M. Brahlek, M. Gazda, V. Keppens, A. R. Mazza, S. J. McCormack, A. Mielewczynski, B. Musico, K. Page, C. M. Rost, S. B. Sinnott, C. Toher, T. Z. Ward and A. Yamamoto, *APL Materials*, 2022, **10**, 110902.
2. X. Liu, Y. Xing, K. Xu, H. Zhang, M. Gong, Q. Jia, S. Zhang and W. Lei, *Small*, 2022, **18**, 2200524.
3. E. Lökçü, Ç. Toparlı and M. Anik, *ACS Applied Materials & Interfaces*, 2020, **12**, 23860-23866.
4. C. Duan, K. Tian, X. Li, D. Wang, H. Sun, R. Zheng, Z. Wang and Y. Liu, *Ceramics International*, 2021, **47**, 32025-32032.
5. K.-H. Tian, C.-Q. Duan, Q. Ma, X.-L. Li, Z.-Y. Wang, H.-Y. Sun, S.-H. Luo, D. Wang and Y.-G. Liu, *Rare Metals*, 2022, **41**, 1265-1275.
6. B. Petrovičová, W. Xu, M. G. Musolino, F. Pantò, S. Patanè, N. Pinna, S. Santangelo and C. Triolo, *Applied Sciences*, 2022, **12**, 5965.
7. B. Xiao, G. Wu, T. Wang, Z. Wei, Y. Sui, B. Shen, J. Qi, F. Wei, Q. Meng, Y. Ren, X. Xue, J. Zheng, J. Mao and K. Dai, *Ceramics International*, 2021, **47**, 33972-33977.
8. H. Chen, N. Qiu, B. Wu, Z. Yang, S. Sun and Y. Wang, *RSC Advances*, 2020, **10**, 9736-9744.
9. T. X. Nguyen, C.-C. Tsai, J. Patra, O. Clemens, J.-K. Chang and J.-M. Ting, *Chemical Engineering Journal*, 2022, **430**, 132658.
10. T. X. Nguyen, J. Patra, C.-C. Tsai, W.-Y. Xuan, H.-Y. T. Chen, M. S. Dyer, O. Clemens, J. Li, S. B. Majumder, J.-K. Chang and J.-M. Ting, *Advanced Functional Materials*, 2023, **33**, 2300509.
11. J. Patra, T. X. Nguyen, C.-C. Tsai, O. Clemens, J. Li, P. Pal, W. K. Chan, C.-H. Lee, H.-Y. T. Chen, J.-M. Ting and J.-K. Chang, *Advanced Functional Materials*, 2022, **32**, 2110992.